Supplementary information for the paper "Topological Graphene plasmons in a plasmonic realization of the Su-Schrieffer-Heeger Model"

Tatiana G. Rappoport,[1,2] Yuliy V. Bludov,[3] Frank H. L. Koppens,[4,5] and Nuno M. R. Peres[3,6]

[1]*Instituto de Telecomunicações, Instituto Superior Técnico, University of Lisbon, Avenida Rovisco Pais 1, Lisboa, 1049001 Portugal*
[2]*Instituto de Física, Universidade Federal do Rio de Janeiro, Caixa Postal 68528, 21941-972 Rio de Janeiro RJ, Brazil*
[3]*Department and Centre of Physics, and QuantaLab, University of Minho, Campus of Gualtar, 4710-057, Braga, Portugal*
[4]*ICFO-Institut de Ciencies Fotoniques, The Barcelona Institute of Science and Technology, 08860 Castelldefels (Barcelona), Spain*
[5]*ICREA-Institució Catalana de Recerca i Estudis Avançats, Barcelona, Spain*
[6]*International Iberian Nanotechnology Laboratory (INL), Av. Mestre José Veiga, 4715-330, Braga, Portugal*

I. SEMI-ANALYTICAL APPROACH TO THE MODELLING OF GRAPHENE PLASMONIC CRYSTAL.

We consider the structure, depicted in Fig. 1. The graphene layer is deposited on top of the semi-infinite substrate, which is characterized by the dielectric constant ε_S and occupies the half-space $z > W + d$. From other side the graphene layer is covered with a spacer layer, which dielectric constant and thickness are ε_d and d, respectively. An array of metallics rods (PECs) with cross-section $W \times W$ is deposited on top of the capping layer. The Period consists of two separations of widths a and b, while distances between neibouring rods W are equal. Thus, the period of the structure is equal to $L = 2W + a + b$. In details, slits of width a are arranged at $-(W + a + b)/2 + lL < x < -(W - a + b)/2 + lL$, while slits of width b are arranged at $(W + a - b)/2 + lL < x < (W + a + b)/2 + lL$ (here l is the number of period).

A. Main equations

Assuming electromagnetic field time-dependence as $\mathbf{E}, \mathbf{H} \sim \exp -i\omega t$, we represent Maxwell equations for p-polarized wave as

$$\frac{\partial E_x^{(j)}}{\partial z} - \frac{\partial E_z^{(j)}}{\partial x} = \frac{i\omega}{c} H_y^{(j)}, \tag{1}$$

$$-\frac{\partial H_y^{(j)}}{\partial z} = -\frac{i\omega}{c}\varepsilon^{(j)} E_x^{(j)}, \tag{2}$$

$$\frac{\partial H_y^{(j)}}{\partial x} = -\frac{i\omega}{c}\varepsilon^{(j)} E_z^{(m)}. \tag{3}$$

where ω is wave cyclic frequency, c is the velocity of light in vacuum. The superscripts $j = 1, 2, 3, 4$ correspond to the spatial domains $z < 0$, $0 < z < W$, $W < z < W + d$, and $z > W + d$, respectively. Also for the sake of simplicity we will admit, that the dielectric constant of all media are $\varepsilon^{(j)} = 1$.

In the medium $j = 1$ the solutions of Maxwell equation can be represented as

$$\begin{pmatrix} H_y^{(1)}(x,z) \\ E_x^{(1)}(x,z) \end{pmatrix} = \sum_{m=-\infty}^{\infty} \hat{F}_m \begin{pmatrix} H_y^{(i)} \delta_{m,0} \exp\left[ip_m^{(1)} z\right] \\ H_{y||m}^{(r)} \exp\left[-ip_m^{(1)} z\right] \end{pmatrix} \exp\left[i\left(k_x + \frac{2\pi m}{L}\right)x\right], \tag{4}$$

where

$$\hat{F}_m = \begin{pmatrix} 1 & 1 \\ \frac{cp_m}{\omega} & -\frac{cp_m}{\omega} \end{pmatrix} \text{ is the field matrix, and } p_m = \sqrt{\left(\frac{\omega}{c}\right)^2 - \left(k_x + \frac{2\pi m}{L}\right)^2}$$

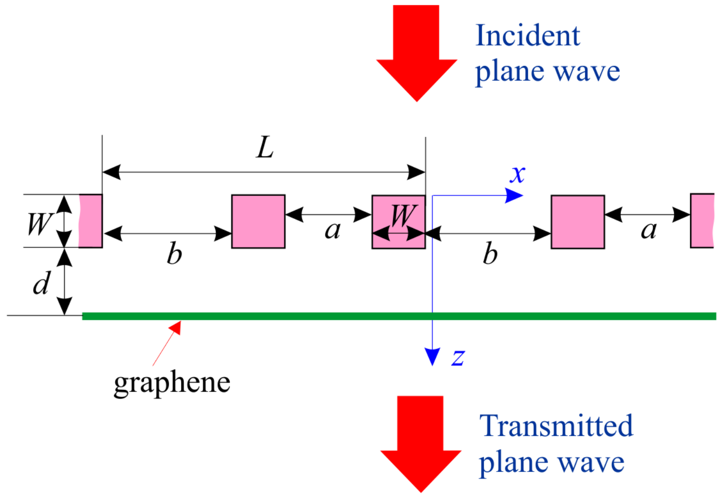

FIG. 1. Geometry of problem: diffraction grating made of PEC, arranged above the graphene monolayer.

is the out-of-plane wavevector component of mth harmonics, $H_y^{(i)}$ and $H_{y||m}^{(r)}$ are the amplitudes of the magnetic field of incident and reflected wave of mth harmonics, k_x is the in-plane wavevector component of incident wave. Incide the substrate, $j=4$, the electromagnetic field can be expressed as

$$\begin{pmatrix} H_y^{(4)}(x,z) \\ E_x^{(4)}(x,z) \end{pmatrix} = \sum_{m=-\infty}^{\infty} \hat{F}_m \begin{pmatrix} H_y^{(t)} \exp\left[ip_m (z-W-d)\right] \\ 0 \end{pmatrix} \exp\left[i\left(k_x + \frac{2\pi m}{L}\right)x\right]. \tag{5}$$

$$\tag{6}$$

In Eq. (5) zero in the second line means absence of the backward-propagating waves. Inside the finite medium $j=3$ electromagnetic fields can be represented in form of the transfer-matrix

$$\hat{Q}_m(z) = \begin{pmatrix} \cos\left[p_m z\right] & \frac{i\omega}{cp_m}\sin\left[p_m z\right] \\ \frac{icp_m}{\omega}\sin\left[p_m z\right] & \cos\left[p_m z\right] \end{pmatrix},$$

i.e.

$$\begin{pmatrix} H_y^{(3)}(x,z) \\ E_x^{(3)}(x,z) \end{pmatrix} = \sum_{m=-\infty}^{\infty} \hat{Q}_m(z-W-d) \begin{pmatrix} h_{y||m}^{(3)}(W+d) \\ e_{x||m}^{(3)}(W+d) \end{pmatrix} \exp\left[i\left(k_x + \frac{2\pi m}{L}\right)x\right].$$

Electromagnetic fields across the graphene are linked through the boundary conditions, namely

$$\begin{pmatrix} h_{y||m}^{(3)}(W+d) \\ e_{x||m}^{(3)}(W+d) \end{pmatrix} = \hat{Q}_g \begin{pmatrix} h_{y||m}^{(4)}(W+d) \\ e_{x||m}^{(4)}(W+d) \end{pmatrix} \tag{7}$$

with the matrix

$$\hat{Q}_m^{(g)} = \begin{pmatrix} 1 & \frac{4\pi}{c}\sigma_g(\omega) \\ 0 & 1 \end{pmatrix}.$$

Here $\sigma_g(\omega)$ is the Drude-like expression for graphene's conductivity, whose form is given in the main text. If this boundary condition is applied, one can obtain the expression for the electromagnetic fields at $z=W$ as

$$\begin{pmatrix} H_y^{(3)}(x,W) \\ E_x^{(3)}(x,W) \end{pmatrix} = \sum_{m=-\infty}^{\infty} \hat{F}_m^{(tot)} \begin{pmatrix} H_y^{(t)} \\ 0 \end{pmatrix} \exp\left[i\left(k_x + \frac{2\pi m}{L}\right)x\right], \tag{8}$$

where

$$\hat{F}_m^{(tot)} = \hat{Q}_m\left(-d\right)\hat{Q}_m^{(g)}\hat{F}_m$$

is the total field matrix.

In the medium $j = 2$, the electromagnetic field can be represented as the superposition of waveguide modes inside the slits. Thus, inside the spatial domain $-\left(W+a+b\right)/2+lL < x < -\left(W-a+b\right)/2+lL$ (slits of width a) the tangential components of the electromagnetic field can be written as

$$\begin{pmatrix} H_{y||l}^{(2,a)}(x,z) \\ E_{x||l}^{(2,a)}(x,z) \end{pmatrix} = ia\sum_{n=0}^{\infty}\cos\left[\frac{n\pi}{a}\left(x+\frac{W+a+b}{2}-lL\right)\right]\times \begin{pmatrix} \omega/c & \omega/c \\ \nu_n^{(a)} & -\nu_n^{(a)} \end{pmatrix}\begin{pmatrix} A_n^{(+,l)}\exp\left[i\nu_n^{(a)}z\right] \\ A_n^{(-,l)}\exp\left[-i\nu_n^{(a)}\left(z-W\right)\right] \end{pmatrix}, \tag{9}$$

where $\nu_n^{(a)} = \sqrt{\left(\frac{\omega}{c}\right)^2-\left(\frac{n\pi}{a}\right)^2}$, l is the number of period, $A_n^{(\pm,l)}$ are the amplitudes of forward- and backward-propagating waves of the nth eigenmode in the lth slit. In the similar manner, inside the spatial domain $\left(W+a-b\right)/2+lL < x < \left(W+a+b\right)/2+lL$ (slits of width b) the tangential component of the electromagnetic waves are

$$\begin{pmatrix} H_{y||l}^{(2,b)}(x,z) \\ E_{x||l}^{(2,b)}(x,z) \end{pmatrix} = ib\sum_{n=0}^{\infty}\cos\left[\frac{n\pi}{b}\left(x-\frac{W+a-b}{2}-lL\right)\right]\times \begin{pmatrix} \omega/c & \omega/c \\ \nu_n^{(b)} & -\nu_n^{(b)} \end{pmatrix}\begin{pmatrix} B_n^{(+,l)}\exp\left[i\nu_n^{(b)}z\right] \\ B_n^{(-,l)}\exp\left[-i\nu_n^{(b)}\left(z-W\right)\right] \end{pmatrix}. \tag{10}$$

Here $\nu_n^{(b)} = \sqrt{\left(\frac{\omega}{c}\right)^2-\left(\frac{n\pi}{b}\right)^2}$, $B_n^{(\pm,l)}$ stand for the amplitudes of forward- and backward-propagating waves of the nth eigenmode in slit l. Matching the boundary conditions at the surfaces of the metal film $z = 0$ and $z = W$ (continuity of the tangential components of the electric and magnetic fields at slits and condition $E_x \equiv 0$ beyond the slits, details can be found in Ref. [1]), and using the Bloch theorem $A_n^{(\pm,l)} = A_n^{(\pm,l)}\exp\left(ik_xlL\right)$, $B_n^{(\pm,l)} = B_n^{(\pm,0)}\exp\left(ik_xlL\right)$, it is possible to obtain the matrix equations for the amplitudes of the waveguides modes,

$$\sum_{n=0}^{\infty}\hat{U}_{n',n}\begin{pmatrix} A_n^{(+,0)} \\ A_n^{(-,0)} \\ B_n^{(+,0)} \\ B_n^{(-,0)} \end{pmatrix} = \left[\left(\hat{F}_0\right)_{11} - \frac{\left(\hat{F}_0\right)_{21}\left(\hat{F}_0\right)_{12}}{\left(\hat{F}_0\right)_{22}}\right]H_y^{(i)}\begin{pmatrix} \overline{P_{n'||k_x}^{(a)}} \\ P_{n'||k_x}^{(b)} \\ 0 \\ 0 \end{pmatrix}.$$

Here elements of matrix $\hat{U}_{n',n}$ can be represented as

$$\left(\hat{U}_{n',n}\right)_{11} = \delta_{n',n}\frac{1+\delta_{n',0}}{2}\frac{i\omega}{c}a - \frac{ia^2}{L}\nu_n^{(a)}\sum_{m=-\infty}^{\infty}\frac{\left(\hat{F}_m\right)_{12}}{\left(\hat{F}_m\right)_{22}}P^{(a)}_{n||k_x+2\pi m/L}\overline{P^{(a)}_{n'||k_x+2\pi m/L}},$$

$$\left(\hat{U}_{n',n}\right)_{12} = \exp\left[i\nu_n^{(a)}W\right]\left\{\delta_{n',n}\frac{1+\delta_{n',0}}{2}\frac{i\omega}{c}a + \frac{ia^2}{L}\nu_n^{(a)}\sum_{m=-\infty}^{\infty}\frac{\left(\hat{F}_m\right)_{12}}{\left(\hat{F}_m\right)_{22}}P^{(a)}_{n||k_x+2\pi m/L}\overline{P^{(a)}_{n'||k_x+2\pi m/L}}\right\},$$

$$\left(\hat{U}_{n',n}\right)_{13} = -\frac{ib^2}{L}\nu_n^{(b)}\sum_{m=-\infty}^{\infty}\frac{\left(\hat{F}_m\right)_{12}}{\left(\hat{F}_m\right)_{22}}P^{(b)}_{n||k_x+2\pi m/L}\overline{P^{(a)}_{n'||k_x+2\pi m/L}},$$

$$\left(\hat{U}_{n',n}\right)_{14} = -\exp\left[i\nu_n^{(b)}W\right]\left(\hat{U}_{n',n}\right)_{13},$$

$$\left(\hat{U}_{n',n}\right)_{21} = -\frac{ia^2}{L}\nu_n^{(a)}\sum_{m=-\infty}^{\infty}\frac{\left(\hat{F}_m\right)_{12}}{\left(\hat{F}_m\right)_{22}}P^{(a)}_{n||k_x+2\pi m/L}\overline{P^{(b)}_{n'||k_x+2\pi m/L}},$$

$$\left(\hat{U}_{n',n}\right)_{22} = -\exp\left[i\nu_n^{(a)}W\right]\left(\hat{U}_{n',n}\right)_{21},$$

$$\left(\hat{U}_{n',n}\right)_{23} = \delta_{n',n}\frac{1+\delta_{n',0}}{2}\frac{i\omega}{c}b - \frac{ib^2}{L}\nu_n^{(b)}\sum_{m=-\infty}^{\infty}\frac{\left(\hat{F}_m\right)_{12}}{\left(\hat{F}_m\right)_{22}}P^{(b)}_{n||k_x+2\pi m/L}\overline{P^{(b)}_{n'||k_x+2\pi m/L}},$$

$$\left(\hat{U}_{n',n}\right)_{24} = \exp\left[i\nu_n^{(b)}W\right]\left\{\delta_{n',n}\frac{1+\delta_{n',0}}{2}\frac{i\omega}{c}b + \frac{ib^2}{L}\nu_n^{(b)}\sum_{m=-\infty}^{\infty}\frac{\left(\hat{F}_m\right)_{12}}{\left(\hat{F}_m\right)_{22}}P^{(b)}_{n||k_x+2\pi m/L}\overline{P^{(b)}_{n'||k_x+2\pi m/L}}\right\},$$

$$\left(\hat{U}_{n',n}\right)_{31} = \exp\left[i\nu_n^{(a)}W\right]\left\{\delta_{n',n}\frac{1+\delta_{n',0}}{2}\frac{i\omega}{c}a - \frac{ia^2}{L}\nu_n^{(a)}\sum_{m=-\infty}^{\infty}\frac{\left(\hat{F}_m^{(tot)}\right)_{11}}{\left(\hat{F}_m^{(tot)}\right)_{21}}P^{(a)}_{n||k_x+2\pi m/L}\overline{P^{(a)}_{n'||k_x+2\pi m/L}}\right\},$$

$$\left(\hat{U}_{n',n}\right)_{32} = \delta_{n',n}\frac{1+\delta_{n',0}}{2}\frac{i\omega}{c}a + \frac{ia^2}{L}\nu_n^{(a)}\sum_{m=-\infty}^{\infty}\frac{\left(\hat{F}_m^{(tot)}\right)_{11}}{\left(\hat{F}_m^{(tot)}\right)_{21}}P^{(a)}_{n||k_x+2\pi m/L}\overline{P^{(a)}_{n'||k_x+2\pi m/L}},$$

$$\left(\hat{U}_{n',n}\right)_{34} = \frac{ib^2}{L}\sum_{n=0}^{\infty}\nu_n^{(b)}\sum_{m=-\infty}^{\infty}\frac{\left(\hat{F}_m^{(tot)}\right)_{11}}{\left(\hat{F}_m^{(tot)}\right)_{21}}P^{(b)}_{n||k_x+2\pi m/L}\overline{P^{(a)}_{n'||k_x+2\pi m/L}},$$

$$\left(\hat{U}_{n',n}\right)_{33} = -\exp\left[i\nu_n^{(b)}W\right]\left(\hat{U}_{n',n}\right)_{34},$$

$$\left(\hat{U}_{n',n}\right)_{42}=\frac{ia^2}{L}\nu_n^{(a)}\sum_{m=-\infty}^{\infty}\frac{\left(\hat{F}_m^{(tot)}\right)_{11}}{\left(\hat{F}_m^{(tot)}\right)_{21}}P^{(a)}_{n||k_x+2\pi m/L}\overline{P^{(b)}_{n'||k_x+2\pi m/L}},$$

$$\left(\hat{U}_{n',n}\right)_{41}=-\exp\left[i\nu_n^{(a)}W\right]\left(\hat{U}_{n',n}\right)_{42},$$

$$\left(\hat{U}_{n',n}\right)_{43}=\exp\left[i\nu_n^{(b)}W\right]\left\{\delta_{n',n}\frac{1+\delta_{n',0}}{2}\frac{i\omega}{c}b-\frac{ib^2}{L}\nu_n^{(b)}\sum_{m=-\infty}^{\infty}\frac{\left(\hat{F}_m^{(tot)}\right)_{11}}{\left(\hat{F}_m^{(tot)}\right)_{21}}P^{(b)}_{n||k_x+2\pi m/L}\overline{P^{(b)}_{n'||k_x+2\pi m/L}}\right\},$$

$$\left(\hat{U}_{n',n}\right)_{44}=\delta_{n',n}\frac{1+\delta_{n',0}}{2}\frac{i\omega}{c}b+\frac{ib^2}{L}\nu_n^{(b)}\sum_{m=-\infty}^{\infty}\frac{\left(\hat{F}_m^{(tot)}\right)_{11}}{\left(\hat{F}_m^{(tot)}\right)_{21}}P^{(b)}_{n||k_x+2\pi m/L}\overline{P^{(b)}_{n'||k_x+2\pi m/L}}.$$

The parameters $P^{(a)}_{n||k_x+2\pi m/L}$, $P^{(b)}_{n||k_x+2\pi m/L}$ are different for even and odd n. Namely, when n is even

$$P^{(a)}_{n||k_x+2\pi m/L}=\frac{2}{a}\exp\left[i\frac{W+b}{2}\left(k_x+\frac{2\pi m}{L}\right)\right]\frac{\left(k_x+\frac{2\pi m}{L}\right)\sin\left[\left(k_x+\frac{2\pi m}{L}\right)\frac{a}{2}\right]}{\left(k_x+\frac{2\pi m}{L}\right)^2-\left(\frac{n\pi}{a}\right)^2},$$

$$P^{(b)}_{n||k_x+2\pi m/L}=\frac{2}{b}\exp\left[-i\frac{W+a}{2}\left(k_x+\frac{2\pi m}{L}\right)\right]\frac{\left(k_x+\frac{2\pi m}{L}\right)\sin\left[\left(k_x+\frac{2\pi m}{L}\right)\frac{b}{2}\right]}{\left(k_x+\frac{2\pi m}{L}\right)^2-\left(\frac{n\pi}{b}\right)^2}.$$

For odd n we have

$$P^{(a)}_{n||k_x+2\pi m/L}=\frac{2}{ia}\exp\left[i\frac{W+b}{2}\left(k_x+\frac{2\pi m}{L}\right)\right]\frac{\left(k_x+\frac{2\pi m}{L}\right)\cos\left[\left(k_x+\frac{2\pi m}{L}\right)\frac{a}{2}\right]}{\left(k_x+\frac{2\pi m}{L}\right)^2-\left(\frac{n\pi}{a}\right)^2},$$

$$P^{(b)}_{n||k_x+2\pi m/L}=\frac{2}{ib}\exp\left[-i\frac{W+a}{2}\left(k_x+\frac{2\pi m}{L}\right)\right]\frac{\left(k_x+\frac{2\pi m}{L}\right)\cos\left[\left(k_x+\frac{2\pi m}{L}\right)\frac{b}{2}\right]}{\left(k_x+\frac{2\pi m}{L}\right)^2-\left(\frac{n\pi}{b}\right)^2}.$$

The amplitudes of the reflected and transmitted waves can be obtained from the amplitudes of waveguide modes as

$$H^{(r)}_{y||m}=\frac{1}{\left(\hat{F}_m\right)_{22}}\left[\frac{ia^2}{L}\sum_{n=0}^{\infty}\nu_n^{(a)}P^{(a)}_{n||k_x+2\pi m/L}\left\{A_n^{(+,0)}-A_n^{(-,0)}\exp\left[i\nu_n^{(a)}W\right]\right\}+\right.$$
$$\left.+\frac{ib^2}{L}\sum_{n=0}^{\infty}\nu_n^{(b)}P^{(b)}_{n||k_x+2\pi m/L}\left\{B_n^{(+,0)}-B_n^{(-,0)}\exp\left[i\nu_n^{(b)}W\right]\right\}-\left(\hat{F}_m^{(1)}\right)_{21}H_y^{(i)}\delta_{m,0}\right], \tag{11}$$

$$H^{(t)}_{y||m}=\frac{1}{\left(\hat{F}_m^{(tot)}\right)_{21}}\left[\frac{ia^2}{L}\sum_{n=0}^{\infty}\nu_n^{(a)}P^{(a)}_{n||k_x+2\pi m/L}\left\{A_n^{(+,0)}\exp\left[i\nu_n^{(a)}W\right]-A_n^{(-,0)}\right\}+\right.$$
$$\left.+\frac{ib^2}{L}\sum_{n=0}^{\infty}\nu_n^{(b)}P^{(b)}_{n||k_x+2\pi m/L}\left\{B_n^{(+,0)}\exp\left[i\nu_n^{(b)}W\right]-B_n^{(-,0)}\right\}\right]. \tag{12}$$

The reflectance and transmittance coefficients can be obtained from Eqs. (11) and (12) as

$$R=\left[p_0\left|H_y^{(i)}\right|^2\right]^{-1}\mathrm{Re}\left\{\sum_{m=-\infty}^{\infty}p_m\left|H^{(r)}_{y||m}\right|^2\right\}, \tag{13}$$

$$T=\left[p_0\left|H_y^{(i)}\right|^2\right]^{-1}\mathrm{Re}\left\{\sum_{m=-\infty}^{\infty}p_m\left|H^{(t)}_{y||m}\right|^2\right\}, \tag{14}$$

whie the loss function is defined as imaginary part of the reflected wave's magnetic field at point $x=0$, divided by incident wave's amplitude, i.e. $\mathrm{Im}\left\{\sum_{m=-\infty}^{\infty}H^{(r)}_{y||m}/H_y^{(i)}\right\}$.

The absorbance $A=1-R-T$ of the considered structure is shown at Fig. 2. As seen, the coincidence between the numerical (dashed lines) and semi-analytical (solid lines) results is excellent. In this figure the absorbance maxima

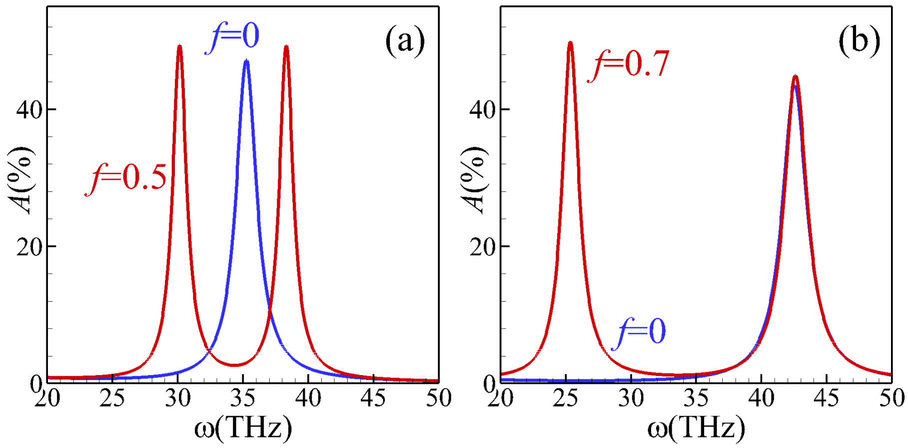

FIG. 2. Absorbance A versus frequency ω of the structure, depicted in Fig. 1 for nornal incidence ($k_x = 0$), calculated by the semi-analytical (solid lines) or numerical (dashed lines) methods. The parameters of the structure in panel (a) are: $E_F = 0.6\,\mathrm{eV}$, $a = 75\,\mathrm{nm}$, $b = 75\,\mathrm{nm}$ (blue lines, which corresponds to $f = 0$), or $a = 112.5\,\mathrm{nm}$, $b = 37.5\,\mathrm{nm}$ (red lines, which corresponds to $f = 0.5$). The dependencies in panel (b) are calculated for the parameters $E_F = 0.4\,\mathrm{eV}$, $a = 10\,\mathrm{nm}$, $b = 10\,\mathrm{nm}$ (blue line, which corresponds to $f = 0$), or $a = 17\,\mathrm{nm}$, $b = 3\,\mathrm{nm}$ (red line, which corresponds to $f = 0.7$). In both panels $W = 75\,\mathrm{nm}$, $d = 3\,\mathrm{nm}$, $\gamma = 3\,\mathrm{meV}$.

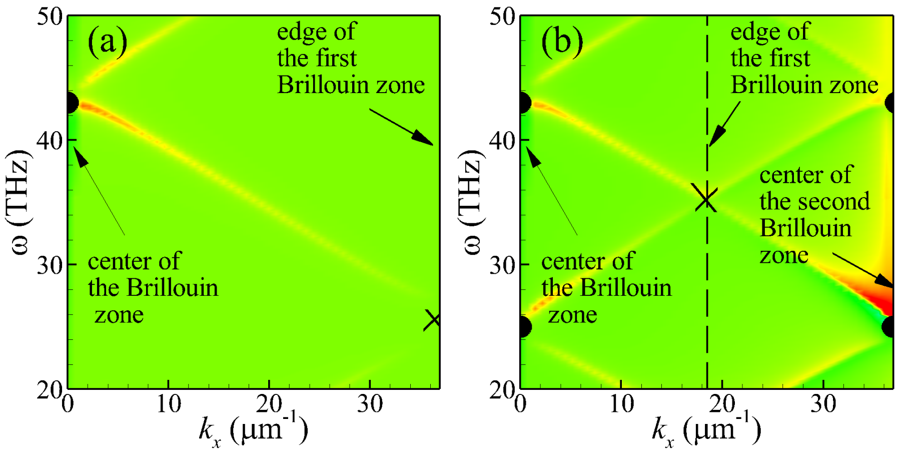

FIG. 3. Loss function (depicted by color map) versus frequency ω and in-plane wavevector k_x for equal values of a and b (a) , or nonequal $a \neq b$ (b). The parameters are the same as in Fig. 2.

correspond to the excitation of surface plasmon-polaritons. In more details, when for some particular frequency ω the in-plane wavevector of one of the diffracted harmonics $k_x + 2\pi m/L$ coincides with the surface plasmon-polariton eigenvalue (obtained from the dispersion relation), the resonant excitation of surface plasmon-polariton takes place. Hence, the energy of incident wave is transformed into the energy of excited surface plasmon-polariton, last fact is revealed in the maximum of absorbance at this particular frequency ω. When widths of the neibouring slits are equal ($a = b$ and, hence, $f = 0$), the spectrum of absorption (blue line) contain one maximum at $\omega \approx 35\,\mathrm{THz}$ [Fig. 2(a)], or $\omega \approx 43\,\mathrm{THz}$ [Fig. 2(b)]. When widths of neibouring peaks are not equal, $a \neq b$ and $f \neq 0$, the high-frequency maximum turns to be blue-shifted (see red lines in Fig. 2), and an additional low-frequency peak at $\omega \approx 30\,\mathrm{THz}$ [Fig. 2(a)], or $\omega \approx 25\,\mathrm{THz}$ [Fig. 2(b)] appears in the spectrum.

When $a = b$, the period of the structure is equal to $D = L/2$. The respective band structure is represented in Fig. 3(a). In this case the center of the first Brillouin zone $k_x = 0$ coincides with left margem of Fig. 3(a), and the edge of the first Brillouin zone $k_x = \pi/D = 2\pi/L \approx 40\,\mu\mathrm{m}^{-1}$ corresponds to the right margem of Fig. 3(a). Also from Fig. 3(a) one can see, that one of the bands starts at frequency $\omega \approx 25\,\mathrm{THz}$ (at $k_x = 2\pi/L$) and ends at $\omega \approx 43\,\mathrm{THz}$ (at $k_x = 0$). For normal incidence it is possible to excite the mode, which corresponds to the crossing of band structure with scanlines $k_x = 2\pi m/D$ (here m is integer). In other words, due to the periodicity of band structure with period

$2\pi/D$ it is possible to excite modes, which lie at center of the first Brillouin zone. Modes at the edge of the first Brillouin zone can not be excited at normal incidence. As a result, mode at $\omega \approx 43\,\mathrm{THz}$ (depicted by the filled circle) can be excited, but mode at $\omega \approx 25\,\mathrm{THz}$ (depicted by cross) can not be excited at normal incidence. This results in only one absorption peak, like depicted by blue lines in Fig. 2.

When $a \neq b$, the period of the structure is equal to $D = L$. The respective band structure is represented in Fig. 3(b). In this case the center of the first Brillouin zone $k_x = 0$ coincides with left margem of the panel, but the edge of the first Brillouin zone $\pi/D = \pi/L \approx 20\,\mu\mathrm{m}^{-1}$ corresponds to the center of Fig. 3(b). Right margem of Fig. 3(b), $k_x = 2\pi/L \approx 40\,\mu\mathrm{m}^{-1}$ corresponds to the center of second Brillouin zone. As one can see, nonequality of neibouring slits leads to the band folding: now band edge $\omega \approx 25\,\mathrm{THz}$ as well as that $\omega \approx 43\,\mathrm{THz}$ lie at the center of the first Brillouin zone and both can be excited at normal incidence, which explains two peaks at Fig. 2, when $a \neq b$ (red lines).

II. NUMERICAL CALCULATIONS

The numerical simulations were implemented in COMSOL Multiphysics, a finite element method solver. Three different types of simulations are performed within the wave optics module. Graphene was simulated as a 2D surface with a Drude like optical conductivity. For all the presented numerical calculations, the relaxation rate of graphene's optical conductivity is set to γ=3 meV.

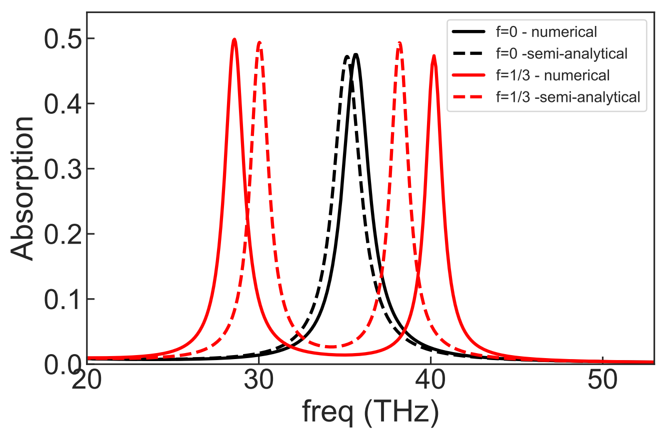

FIG. 4. Comparison between the absorption spectra of the numerical calculations (solid-line) and semi-analytical calculations (dashed-line) for f=0 (black) and f=-2/3 (red)

For the periodic structures, the setup includes Floquet periodic boundary conditions. For the band-structure, we used the eigenfrequency analysis. To avoid excessive numerical issues with the non-linearity of the equations, for the eigenfrequency calculations we considered a lossless version of silver. The numerical and semi-analytical spectra were shifted by a constant wave-length λ_0. The numerical spectra was then adjusted according to the semi-analytical data, which was also consistent with the numerical absorption spectra.

For the Zak phase calculations, we considered a periodic system with Floquet k vectors covering the 1st Brillouin zone. The eigen-fields for each k and $z = z_0$ were then used for the calculation described in the main text. To obtain the periodic part of the electric field, it was multiplied by $e^{(-kx)}$. For the absorption calculations A periodic port excites a TM electromagnetic wave and the total transmission, reflection and absorption are calculated. For the finite systems, PEC boundaries are considered, instead of the periodic boundary conditions.

III. ADDITIONAL FIGURES

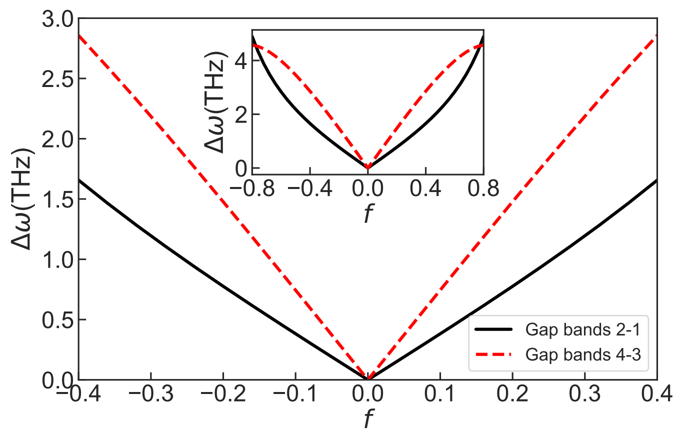

FIG. 5. Linear variation of the gap $\Delta\omega$ between the plasmonic bands 1- 2 (solid line) and 3-4 (dashed line) as a function of f for small values of f. The inset shows $\Delta\omega \times f$ for $f = [-0.8, 0.8]$.

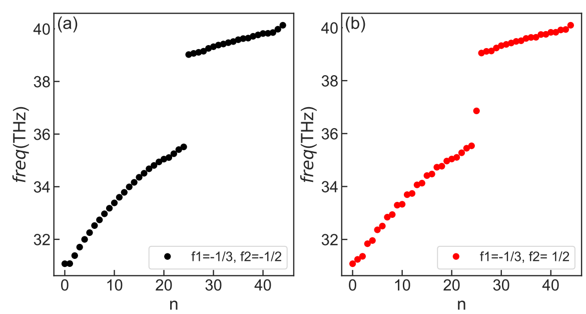

FIG. 6. Energy spectrum of a finite system containing (a) 20 unit cells with f_1=-2/3 and 20 unit cells with f_2=-1/2 and (b) 20 unit cells with f_1=-2/3 and 20 unit cells with $f = 1/2$. For sgn(f_1)=sgn(f_1), the system does not have mid-gap states. For sgn(f_1) $\neq$ sgn(f_1) the system presents a mid-gap state.

[1] Yuliy V. Bludov, Nuno M. R. Peres, and Mikhail I. Vasilevskiy. Excitation of localized graphene plasmons by a metallic slit. *Physical Review B*, 101(7):075415, feb 2020.